

# Propagation mechanisms of guided streamers in plasma jets: the influence of electronegativity of the surrounding gas

Ansgar Schmidt-Bleker<sup>1</sup>, Seth A Norberg<sup>2</sup>, Jörn Winter<sup>1</sup>, Eric Johnsen<sup>2</sup>, S Reuter<sup>1</sup>, K D Weltmann<sup>1</sup> and Mark J Kushner<sup>3</sup>

<sup>1</sup> Leibniz Institute for Plasma Science and Technology e.V. (INP Greifswald) and ZIK plasmatis, Felix-Hausdorff Straße 2, 17489 Greifswald, Germany

<sup>2</sup> Department of Mechanical Engineering, University of Michigan, 2350 Hayward Street, Ann Arbor, MI 48109-2125 USA

<sup>3</sup> Department of Electrical Engineering and Computer Science, University of Michigan, 1301 Beal Avenue, Ann Arbor, MI 48109-2122, USA

E-mail: [stephan.reuter@inp-greifswald.de](mailto:stephan.reuter@inp-greifswald.de) and [mjkush@umich.edu](mailto:mjkush@umich.edu)

Received 7 February 2015, revised 7 April 2015

Accepted for publication 21 April 2015

Published 5 June 2015



CrossMark

## Abstract

Atmospheric pressure plasma jets for biomedical applications are often sustained in He with small amounts of, for example, O<sub>2</sub> impurities and typically propagate into ambient air. The resulting poorly controlled generation of reactive species has motivated the use of gas shields to control the interaction of the plasma plume with the ambient gas. The use of different gases in the shield yields different behavior in the plasma plume. In this paper, we discuss results from experimental and computational investigations of He plasma jets having attaching and non-attaching gas shields. We found that negative ion formation in the He-air mixing region significantly affects the ionization wave dynamics and promotes the propagation of negative guided streamers through an electrostatic focusing mechanism. Results from standard and phase resolved optical emission spectroscopy ratios of emission from states of N<sub>2</sub> and He imply different electric fields in the plasma plume depending on the composition of the shielding gas. These effects are attributed to the conductivity in the transition region between the plasma plume and the shield gas, and the immobile charge represented by negative ions. The lower conductivity in the attaching mixtures enables more extended penetration of the electric field whereas the negative ions aid in focusing the electrons towards the axis.

Keywords: Atmospheric pressure plasma jets, guided ionization waves, phase resolved optical emission spectroscopy, modeling

(Some figures may appear in colour only in the online journal)

## 1. Introduction

Cold atmospheric plasma jets (CAPJ) emanating into ambient air are being investigated for a wide range of biomedical and biotechnological applications [1–3]. The typical CAPJ consists of a rare gas seeded with a small fraction of reactive gas, usually less than a few percent, flowed through a tube of up to a few mm in diameter [4, 5]. Pulse periodic electric discharges in the tube produce an ionized, radical and excited state laden

plume, which subsequently mixes with and reacts with the ambient air. The plasma component of the plume takes the form of periodic ionization waves through the more easily ionized rare-gas dominated channel that is bounded by the less easily ionized ambient gas. The plasma plume is therefore often referred to as a guided streamer. The reactive oxygen and nitrogen species (RONS) produced by CAPJ having guided streamers can be influenced by gas curtains of defined composition surrounding the plume of the plasma jet [6, 7]. Such

control has enabled making correlations of plasma-generated reactive species with biological effects [8, 9].

The effect of the surrounding gas on the plasma propagation and formation of RONS has previously been investigated using helium (He) jets emanating into ambient air and in He atmospheres. Plasma jets using sinusoidally excited needle-shaped electrodes [10] and positive pulses [11] emanating into He atmospheres produce a diffuse discharge due to the ability of the discharge to freely propagate into the ambient gas. When emanating into an air atmosphere, the confining effects of the electronegative and low ionization rate molecular gas surrounding the plume produce a guided streamer. Simulations of a He plasma jet produced similar trends [12].

Several modelling studies have investigated the mechanisms leading to the formation of guided streamers in He-operated plasma jets. Sakiyama and Graves simulated a He plasma jet flowing into nitrogen ( $N_2$ ) impinging on a glass plate with a grounded metal plate underneath [13]. They were able to explain the ring shaped emission patterns and bacteria killing patterns experimentally observed [14] by mixing of excited and ionized He with the surrounding  $N_2$ . Naidis also found annular emission patterns in a simulation including both  $N_2$  and oxygen ( $O_2$ ) as the surrounding gas [15]. He found that in regions where the mole fraction of air exceeded 0.1%, attachment to  $O_2$  prevented further radial expansion of the streamer. Detachment from  $O_2^-$  formed in a previous pulse can provide seed electrons for the propagation of the subsequent streamer. The numerical investigation of Breden *et al* showed that while photoionization in front of the streamer head does increase the propagation speed of guided streamers, it is not a necessary requirement for streamer propagation [12]. They also found that molecular impurities ( $N_2$ ,  $O_2$ , air) of up to 1% can enhance the development of the streamer within the discharge tube while possibly quenching the streamer outside the tube. Several numerical studies have suggested that a finite mixing layer between He and air is not a necessary requirement for the development of a guided streamer [12, 16, 17]. The guiding of streamers by the He gas flow is usually explained by the lower electric fields required for the streamer propagation in He than in the surrounding gas, as well as memory effects such as preionization and accumulation of excited species from the preceding streamer [11, 18].

Naidis [19] investigated the differences between guided streamers created by positive and negative voltage pulses of the same magnitude and found that positive streamers lead to a stronger electric field in the streamer head and tend to propagate faster and further than negative ones. The emission patterns found in that work agreed well with experiments [20]. A comparison of positive and negative streamers was also made by Xiong and Kushner for ionization waves propagating inside dielectric tubes [21]. Unlike guided streamers into ambient gas, it was found that negative streamers propagate faster than positive streamers, an effect attributed to the focusing effect of the tube walls. While in a free jet, electron diffusion leads to a broadening of the streamer head, and consequently to lower electric fields and a slower propagation as found for streamers in air [22], the walls of the tube can rapidly charge and produce an electric field pointing in the direction of streamer propagation.

Winter *et al* [23] measured metastable He ( $He(2^3S_1)$ ,  $He_m$ ) concentrations using laser absorption spectroscopy on a CAPJ while incorporating shielding gases consisting of mixtures of  $N_2$  and  $O_2$ . It was found that the  $He_m$  concentration in the plume strongly depends on the composition of the shielding gas: The  $He_m$  density in the vicinity of the jet nozzle amounts to  $10^{13} \text{cm}^{-3}$  if the  $O_2$  concentration in the shielding is between 15% and 100%. As the  $O_2$  content in the shielding gas is decreased below 10% the  $He_m$  density drops by at least two orders of magnitude (below the detection limit of the system). Similar densities and trends were observed when a mixture of  $O_2$  and Ar was used as the shielding gas. These findings indicate that the decrease in  $He_m$  density with decreasing  $O_2$  content in the shielding gas is not due to the presence of  $N_2$ , but due to the absence of  $O_2$ .

In this paper, we report on the consequences of ambient  $O_2$ —and especially its electronegative properties—on dynamic processes in the plume of a He CAPJ. Several previous investigations have been performed on the particular CAPJ used in this study, the kinpen Sci [24]. For example, the previously mentioned measurements of  $He_m$  densities were made using this device [23]. As a result, the baseline operating characteristics of the CAPJ are well known and can be extrapolated to the broader class of CAPJ [4–6]. The consequences of  $O_2$  content in the ambient and shield were investigated by using optical emission spectroscopy (OES) and numerical modelling. The OES measurements include low-resolution observations of the emission of atomic and molecular lines, high spectral and spatial resolution of  $N_2$  emission bands and time resolved images of the plume of the jet jets using a fast-gating iCCD camera. We found that if the jet is shielded with  $N_2$ , an intense  $N_2$  emission occurs at the side of the jet nozzle and a dark space occurs at a distance of 0.5 to 1 mm from the nozzle. These features do not occur if the jet is shielded by synthetic air. We also observed a backwards directed emission (travelling along the jet axis against the flow direction) during the positive half-cycle if the shielding gas contains  $O_2$ .

Two dimensional numerical modeling of the discharge was also performed. A correlation between the observed emission patterns and the computed electron densities and electric fields was obtained. This leads to the central hypothesis that anions formed from  $O_2$  contribute to a focusing of the electrons in the plume of the jet during the negative half-cycle.

## 2. Description of the experiment and model

### 2.1. Experiment

In this investigation, the plasma jet kinpen Sci was operated with a shielding gas device. The jet is identical to that diagnosed by Winter *et al* [23]. The device features an inner needle electrode which is mounted in the center of a ceramic capillary of 1.6 mm inner diameter with a grounded outer electrode. The inner electrode is driven at a frequency of 940 kHz with a peak-to-peak voltage of 1.7 kV [23]. The jet and shielding gas device are schematically shown in figure 1. The feed gas is He at 2.5 standard liters per minute (slm) (Alphagaz 1, Air

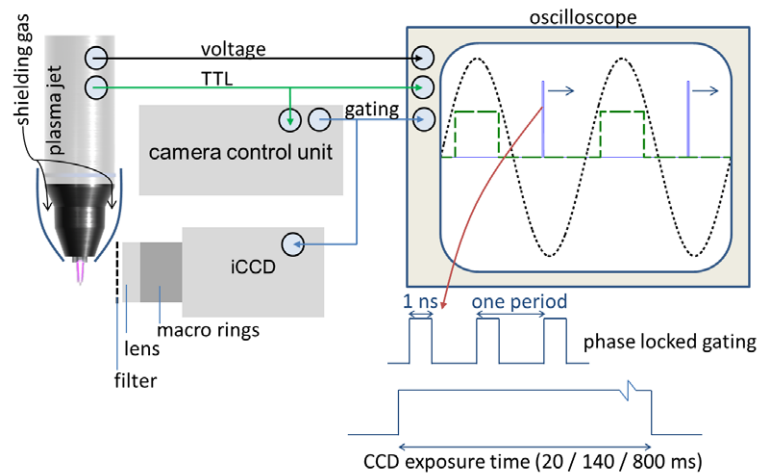


**Figure 1.** Schematics of the experimental setup and principle of the phase resolved optical emission measurements. In the sketch of the oscilloscope, the dotted black line represents the voltage signal, the dashed green line the TTL signal and the continuous blue line the gating signal for the MCP.

Liquide, France). The employed shielding gas mixtures were 5 slm of  $N_2$  and  $O_2$  (Alphagaz 1, Air Liquide, France) in different mixing ratios ranging from pure  $N_2$  to pure  $O_2$ .

Low resolution spectra of the jet emission in the region of 250–970 nm were obtained using the AvaSpec ULS2048X64-2-USB2 (Avantes, Netherlands) spectrometer with a slit width of  $25\mu\text{m}$ . The end-on spectrum was obtained by placing an optical fiber in front of the plume. The spectral sensitivity was calibrated using the light source DH-2000-CAL (Ocean Optics, USA).

Side-on spatially resolved spectra were made with the imaging spectrograph Shamrock 750 (Andor, Northern Ireland) with the EMCCD Newton 971 (Andor) with an entrance slit width of  $20\mu\text{m}$  and a grating with  $600\text{ lines mm}^{-1}$ . Using two lenses, the jet was imaged onto the entrance slit of the spectrometer.

The experimental setup and gating sequence for the PROES measurements are shown in figure 1. A high-repetition rate gated iCCD camera (LaVision PicoStar HR12) was used for the imaging. The image intensifier consists of a photo cathode, micro channel plate (MCP) and phosphor screen. The kinpen Sci generates a TTL signal that is fed to the camera control unit. During each period of the plasma jet the control unit gates the MCP for 1 ns after a fixed phase locked delay with respect to the TTL signal. The gating signal and the voltage applied at the inner electrode of the jet are monitored on the oscilloscope allowing an assignment of the image with the phase of the jet. By varying the delay with respect to the TTL signal phase resolution is obtained. The exposure time of the CCD was adjusted for the light intensity and ranges from 20 ms to 800 ms. A 707 nm filter with a spectral FWHM of 9 nm was used for observing He emission ( $\text{He } 3^3\text{S}-2^3\text{P}$ ) and a 390 nm filter (FWHM 20 nm) was used for  $N_2$  emission (first negative system, FNS and second positive system, SPS). The field of view of the camera for the PROES measurements with the plasma turned off is shown in figure 2. An additional gas flow of 0.1 slm can be introduced in the plume of the plasma jet using a glass pipet.

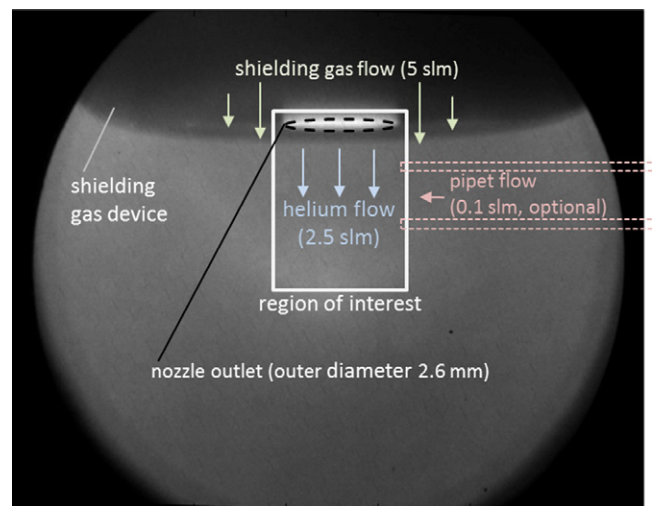


**Figure 2.** Field of view of camera and geometry used in the PROES setup.

## 2.2. Model

Using the 2-D cylindrically symmetric, plasma hydrodynamics model, *non-PDPSIM* [25, 26], a single jet with a shielding gas curtain with dimensions similar to that of the kinpen Sci was simulated using an unstructured triangular mesh as shown in figure 3. The computational domain is 24 mm by 8.8 mm and contains nearly 16000 nodes with 13000 being plasma nodes. The mesh has refinement zones that, as shown in the left panel of figure 3, allow for finer resolution in the discharge region (from  $30\mu\text{m}$  at the tip of the pin electrode) to coarser resolution (0.2 mm) far from the plasma. The primary goal of this computational investigation was to analyze the effects of the shielding gas on the propagation of the ionization wave and the production of reactive species from the interaction of the plasma produced charged and reactive species and the gas in the curtain. A secondary aspect was to validate the model through comparison of trends with the experiment using this

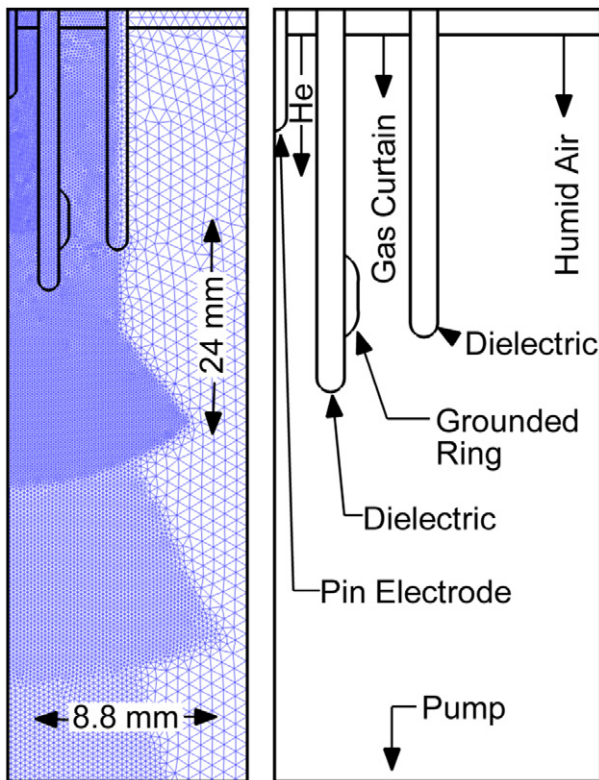


Figure 3. Geometry and mesh applied in the numerical model.

unique scenario of gases shrouding the helium plasma jet to optimize production of RONS.

In this study, the plasma transport module, the radiation transport module and the fluid transport modules of *non-PDPSIM* were used. The neutral flow field was modeled by integrating modified versions of the compressible Navier–Stokes equations which account for large gradients in average molecular weight. The flow field is allowed to develop for 5 ms prior to applying voltage to the electrode. At this point, the plasma transport module is used to solve Poisson’s and charged and neutral species continuity equations with picosecond time-steps using a fully implicit Newton-iteration technique with a maximum allowed error of  $3 \times 10^{-6}$  for convergence for each timestep. Poisson’s equation is solved throughout the entire computational domain, including both dielectric tubes ( $\epsilon/\epsilon_0 = 4$  without conductivity) and electrodes (treated as metal). Using a time-slicing technique, the electron energy equation is updated for electron temperature which is then used to provide transport coefficients and rate coefficients. These coefficients are obtained from tabular stationary solutions of Boltzmann’s equation for the electron energy distributions. These tables are updated every  $5 \times 10^{-11}$  seconds to reflect instantaneous changes in gas composition. Photoionization of  $O_2$  is addressed in the radiation transport module. During the discharge pulse the fluid module is called every  $5 \times 10^{-11}$  seconds to provide close coupling to the plasma transport. The description of the model of an atmospheric pressure plasma jet into humid air is described in depth in [27].

In the numerical investigation, impure He (containing 2 ppm  $O_2$  and 3 ppm  $H_2O$ ) flows through the central tube at

2.5 slm. The shielding gas flows at 5 slm into humid air ( $N_2/O_2/H_2O = 79.5/20/0.5$ ). Four shielding gas compositions were analyzed:  $N_2/O_2 = 99/1$ ,  $1/99$ ,  $80/20$  (synthetic air), and an artificial electronegative  $N_2$  ( $eN_2$ ). In order to isolate the consequences of an electronegative shield, an  $N_2$  shield was modelled while allowing the  $N_2$  to additionally attach to form a fictitious  $N_2^-$  using the same rate of attachment and ion–ion neutralization as would occur for  $O_2^-$ . This is referred to as electronegative  $N_2$  ( $eN_2$ ).

The voltage profile used in the model is a 5 ns rise time to  $-15$  kV and 75 ns duration at that voltage. The ring electrode on the inner tube is grounded. Compared to the experiments, a higher voltage is applied in the model in order to produce a guided streamer on the first discharge pulse. The propagation of a single negative streamer during an 80 ns interval is simulated.

### 3. Results and discussion

#### 3.1. Optical emission spectroscopy

An example of the low resolution optical emission spectrum is shown in figure 4 when using  $N_2$  or synthetic air as the shielding gas. The emission originates from atomic He, the He excimer, atomic oxygen (O), molecular  $N_2$  and molecular  $N_2$  ions, as well as from hydroxyl and atomic hydrogen [28–30]. The end-on spectra obtained with  $N_2$  and synthetic air as shielding gases are similar, which is expected as the emission in this case mainly originates from inside the capillary. Only a slight increase of the intensity of the O lines and a small decrease of the  $N_2$  emission were observed when synthetic air was used compared to  $N_2$ . Note that emission from O, hydroxyl (OH) and atomic hydrogen (H) is observed which originates from impurities in the He. The feed gas contains up to 3 ppm of water vapor and up to 2 ppm of  $O_2$ . Further impurities may result from desorption from the interior surfaces of the feed gas tube, back diffusion from the ambient or diffusion through PTFE tubes [31].

Differences in the spectra for different shielding gases were found when observing the plume from the side, as shown in figure 5. Emission originating from the FNS ( $N_2^+(B) \rightarrow N_2^+(X)$ ) and SPS ( $N_2(C) \rightarrow N_2(B)$ ) of  $N_2$  is shown spatially resolved along the axis of the jet for  $N_2$  and synthetic air shielding gases. In both cases the emission is strongest in the vicinity of the jet nozzle. However, in the  $N_2$ -shielded case, the FNS emission first drops to near zero at around 1 mm and then rises again up to 4.5 mm. Switching from  $N_2$  to synthetic air shielding produces a 50% increase in FNS emission while the SPS emission is nearly totally quenched.

#### 3.2. Effect of shielding gas on ionization wave propagation

The voltage applied at the electrode of the jet is shown in figure 6 together with the total phase resolved emission of the jet along the axis for shielding gas compositions of  $N_2/O_2 = 100/0$ ,  $90/10$ ,  $80/20$  and  $0/100$ . While operating at a carrier frequency of 940 kHz, the voltage signal is additionally modulated at 470 kHz: During a  $2.1 \mu s$  period, the voltage

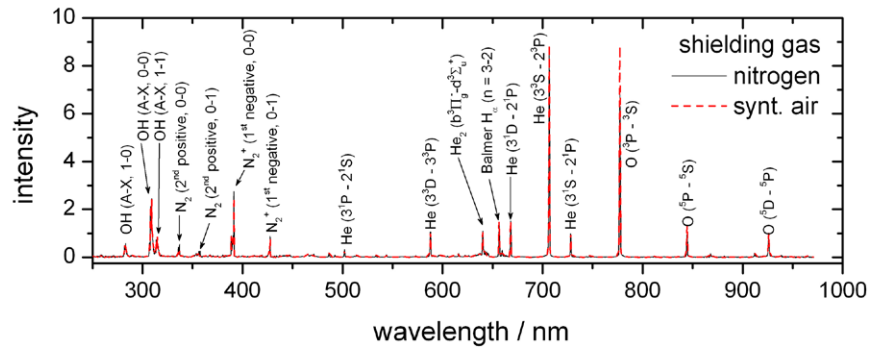


**Figure 4.** End-on spectra when using N<sub>2</sub> or synthetic air as the shielding gas. These spectra do not significantly differ with varying shielding gas composition since the emission dominantly originates in the tube (in contrast to side-on measurements).

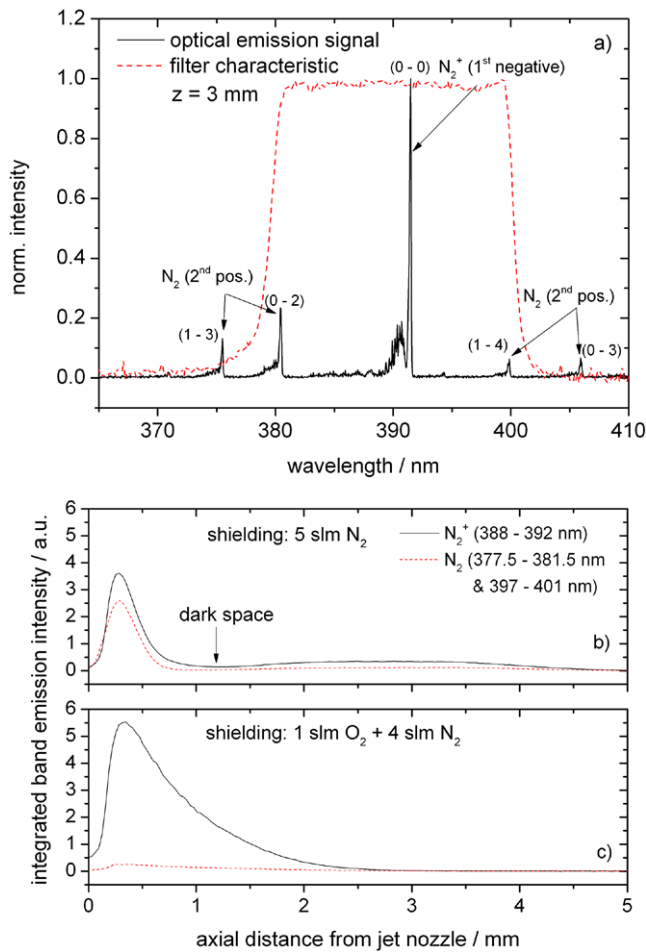


**Figure 5.** (a) Side-on measurement N<sub>2</sub> and N<sub>2</sub><sup>+</sup> emission from the jet operated with N<sub>2</sub> shielding gas. The dashed line shows the transmission curve of the filter used for monitoring the N<sub>2</sub> emission in the PROES measurements. (b) Integrated N<sub>2</sub> and N<sub>2</sub><sup>+</sup> band emission intensity along the axis of the jet for N<sub>2</sub> as the shielding gas. (c) Integrated emission for synthetic air as the shielding gas.

signal has a strong positive half-cycle, followed by a strong negative, a weak positive and a weak negative half-cycle. This pattern is regular with a 2.1 μs period and is reflected in the axial PROES measurements shown in figures 6(b)–(e). The excitation dynamics strongly depend on the O<sub>2</sub> content of the shielding gas. With an N<sub>2</sub> shield, the excitation front

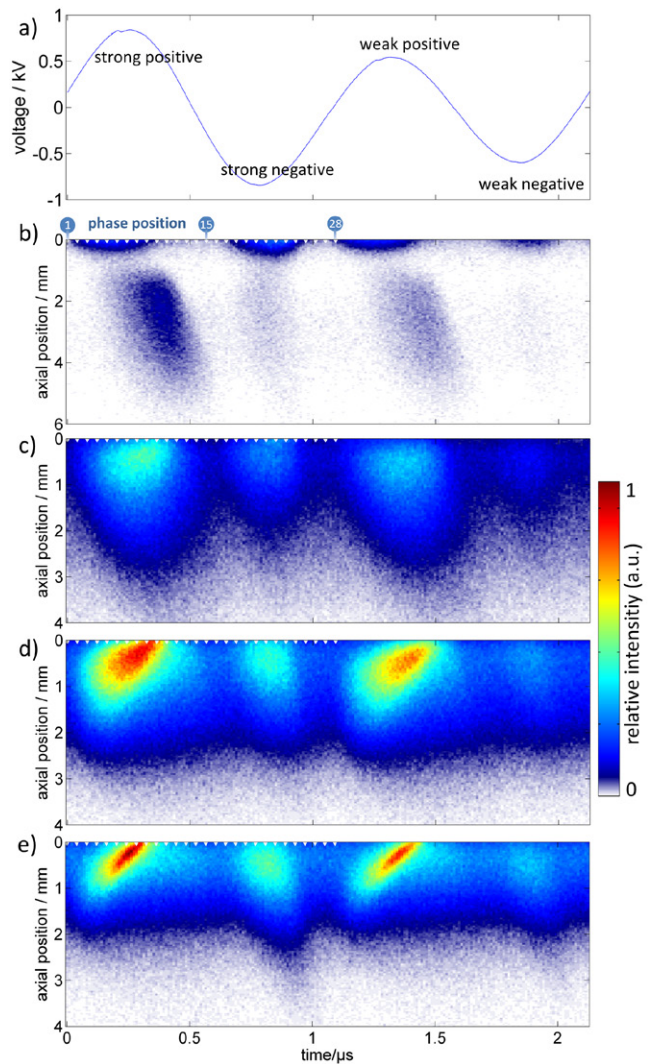


**Figure 6.** Applied voltage (a) and phase resolved on-axis emission without a filter and shielding gases having N<sub>2</sub>/O<sub>2</sub> mixtures of (a) 100/0, (c) 90/10, (d) 80/20 and (e) 0/100. The angles of the emission patterns yield the speed of the excitation fronts. Images in figures 7–10 were taken at phase positions 1–28 shown in (b).

propagates from the nozzle in the direction of the gas flow with a speed of 1800 m s<sup>-1</sup> during the positive half-cycle. The emission features a dark space at a distance of about 0.5 to 1 mm, which is visible to the naked eye. The excitation front

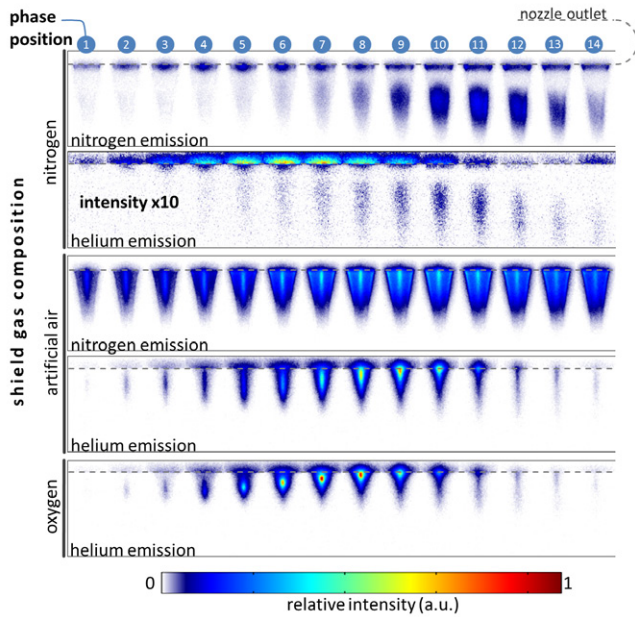


**Figure 7.** N<sub>2</sub> and He emission during the strong positive half-cycle for different shielding gas compositions. The phase positions are chosen as defined in figure 6. Note that the He emission intensity for the N<sub>2</sub> shielding case is multiplied by a factor ten compared to the He emission for the synthetic air and O<sub>2</sub> case.

propagates in the opposite direction with a speed of about  $4200 \text{ m s}^{-1}$  if the shielding gas contains O<sub>2</sub>. The speeds of the forward and the backwards directed excitation waves were obtained from the angle of spatial position versus time in figures 6(b) and (e). The backwards directed excitation wave originates from the plume region and propagates towards the inner needle electrode. It only appears if the shielding gas contains O<sub>2</sub> and is most pronounced if the shielding gas is pure O<sub>2</sub> (see figure 6(e)). Such backwards directed excitation waves have been observed in needle-to-plane discharges [32].

Phase resolved optical emission from He and N<sub>2</sub> is shown in shown in in figure 7 for the strong positive half-cycle and in figure 8 for the strong negative half-cycle. The timings of the images are indicated by the phase number using the scale shown in figure 6(b). The exposure time of the CCD is 140 ms for N<sub>2</sub> emission and 800 ms for He emission. The bandwidth of the filter for the He 706.7 nm line is small enough to dominantly capture this line. The filter used for N<sub>2</sub> emission captures both SPS and FNS radiation (see figure 5(a)).

With N<sub>2</sub> shielding gas, the N<sub>2</sub> emission during the positive half-cycle is low in the plume region. Emission from N<sub>2</sub> is strong from phases 9–13 after which it decays (phase positions 14–28). During the negative half-cycle (phase positions 19–25), strong emission from N<sub>2</sub> occurs at the side of the nozzle outlet. This emission is not followed by an increase in emission at distances further from the nozzle. The ionization wave here appears to spread radially outward rather than being focused in the axial direction.

As O<sub>2</sub> is introduced in the shielding gas, the emission dynamics change. A low but broad N<sub>2</sub> emission occurs throughout the entire period. This emission follows the contours of the ambient air density. A similar fluorescence pattern

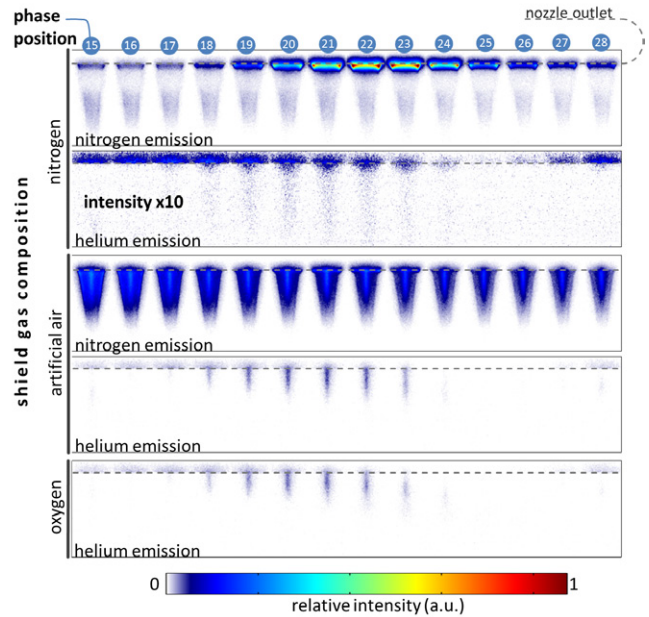


**Figure 8.** Same as figure 7 for the strong negative half-cycle (continued).

was observed in laser induced fluorescence measurements of OH and was explained by diffusion of air into the active plume of the jet [33, 34]. Strong N<sub>2</sub> emission also occurs on-axis during phase 7–12 and at the He-air boundary. Emission maxima at the He-air boundary may result from the higher N<sub>2</sub> densities at this position. The strong on-axis emission directly correlates with the emission from He at these phases. The maximum in He emission propagates from a distance of 2.5 mm towards the nozzle. This behavior occurs at low O<sub>2</sub> concentrations (10%) in the shielding gas and becomes more pronounced as the O<sub>2</sub> content increases. Qualitatively the He emission dynamics are the same for 10–100% O<sub>2</sub> in the shielding gas. The emission dynamics suggest that a backwards directed excitation wave occurs from the plume region towards the anode.

The emission during the negative half-cycle (figure 8) is also qualitatively different when O<sub>2</sub> is present in the shielding gas. The strong N<sub>2</sub> emission at the side of the nozzle with pure N<sub>2</sub> shielding gas does not occur. Instead, He emission is observed on-axis at phase positions 18 to 23 with O<sub>2</sub> in the shield. One explanation is that without O<sub>2</sub> in the shielding gas, high energy electrons propagate in the radial direction where they excite N<sub>2</sub> at the side of the jet nozzle. With O<sub>2</sub> in the shielding gas, these electrons are focused towards the axis and are able to excite the high energy He states.

Both the N<sub>2</sub> FNS ( $\text{N}_2^+(\text{B}) \rightarrow \text{N}_2^+(\text{X})$ ) and the He 706.7 nm emission are more intense if O<sub>2</sub> is in the shielding gas while the FNS emission is stronger without O<sub>2</sub> present (see figures 5, 7 and 8). These trends indicate that the N<sub>2</sub> shielded jet produces lower electric fields (and lower electron energies) than the synthetic air or O<sub>2</sub>-shielded jet. The energy levels involved in the emission of FNS and SPS radiation and He 706.7 nm emission and the rate coefficients for the direct excitation from the ground states are shown in figure 9. The rate coefficients were computed with BOLSIG+ [35] using the cross sections from

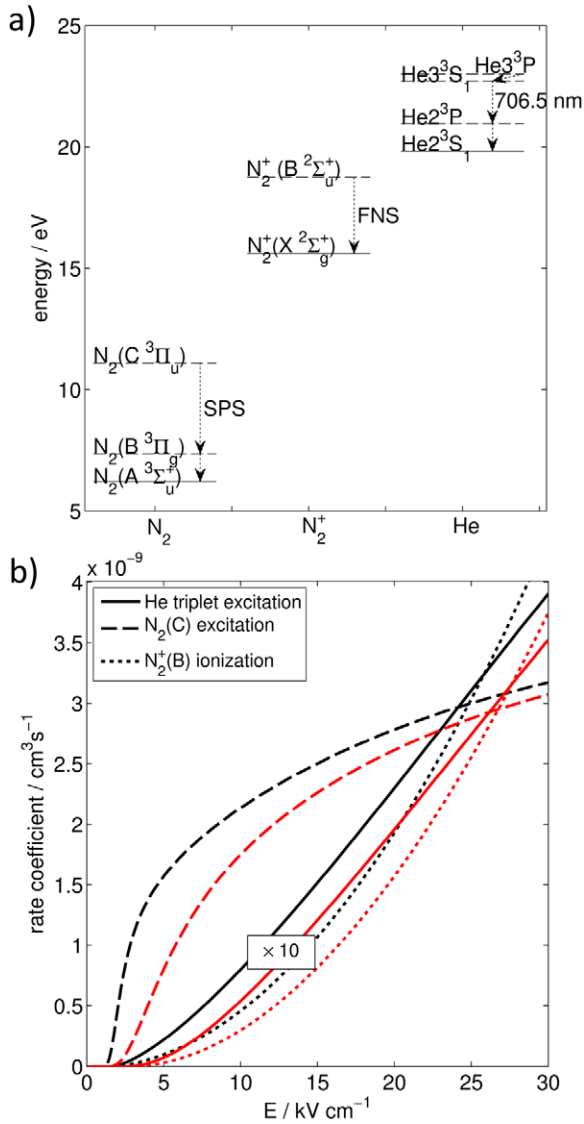


**Figure 9.** (a) Energy levels involved in the FNS and SPS emission from N<sub>2</sub> and He 706.7 nm emission. (b) Electric field-dependent rate coefficients for the excitation of the levels for FNS, SPS and 706.7 nm emission. Rate coefficients are shown for pure He (black lines) and 99% He with 1% dry air (red lines).

[36, 37]. At lower electric fields, more SPS radiation can be expected, while at high electric fields the FNS radiation and He 706.7 nm emission should increase on a relative basis.

### 3.3. Effect of asymmetric O<sub>2</sub> distribution in the plasma plume on ionization wave propagation

To investigate the effect of an electronegative gas in the ambient gas surrounding the jet, gas was injected asymmetrically into the jet using the pipette (see figure 2). A flow of 0.1 slm of either O<sub>2</sub> or N<sub>2</sub> was injected. The average lateral speed of the injected gas was 2 ms<sup>-1</sup> compared to the average speed of the gas through the capillary of 21 ms<sup>-1</sup> and of the shield gas of 3 ms<sup>-1</sup>. He and N<sub>2</sub> emission are shown in figure 10 for the positive half-cycle and figure 11 for the negative half-cycle. When N<sub>2</sub> is flowed through the pipette, there is little change in the emission from either He or N<sub>2</sub>. The additional

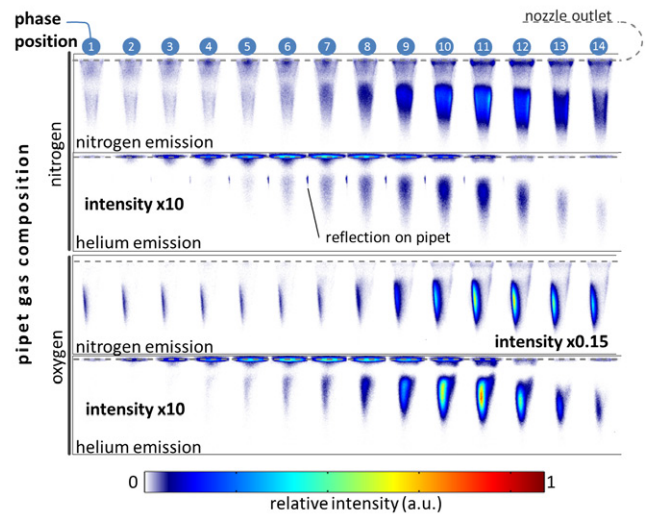


**Figure 10.** N<sub>2</sub> and He emission during the strong positive half-cycle of the N<sub>2</sub>-shielded jet doped with either N<sub>2</sub> or O<sub>2</sub> from a pipette. The phase positions are chosen as defined in figure 6.

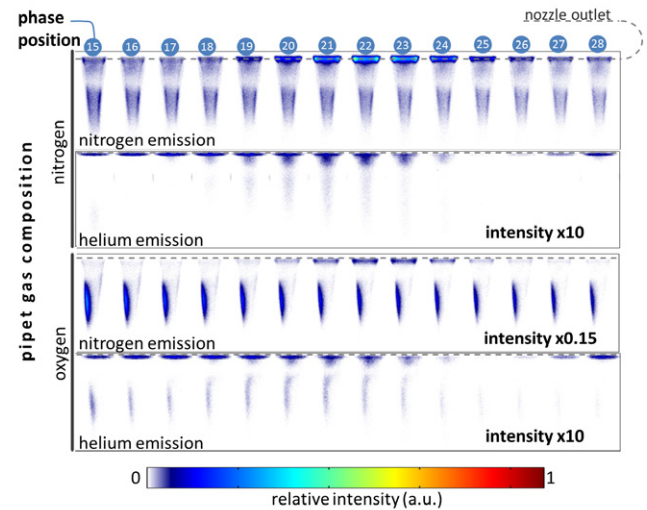


**Figure 11.** Same as figure 10 for the strong negative half-cycle (continued).

gas flow through the pipette does not significantly influence the flow field as the flow remains laminar. However, when O<sub>2</sub> is flowed through the pipette from the right side, a stronger emission from both He and N<sub>2</sub> occurs on the left side of the plume. The overall dynamics are not as significantly changed as when O<sub>2</sub> is in the shielding gas, especially no backwards directed excitation wave is observed during the positive half-cycle. As without the pipet, the emission in the positive half-cycle is stronger than in the negative half-cycle. Qualitatively the results do not depend on the exact position of, or the mass flow through the pipette. The exception is when the flow through the pipette is in the slm range, which resulted in bending of the visible plasma plume due to the crossflow.

From these results, two conclusions may be drawn. First, the differences in the guided streamer dynamics observed when O<sub>2</sub> is present in the shielding gas likely do not result

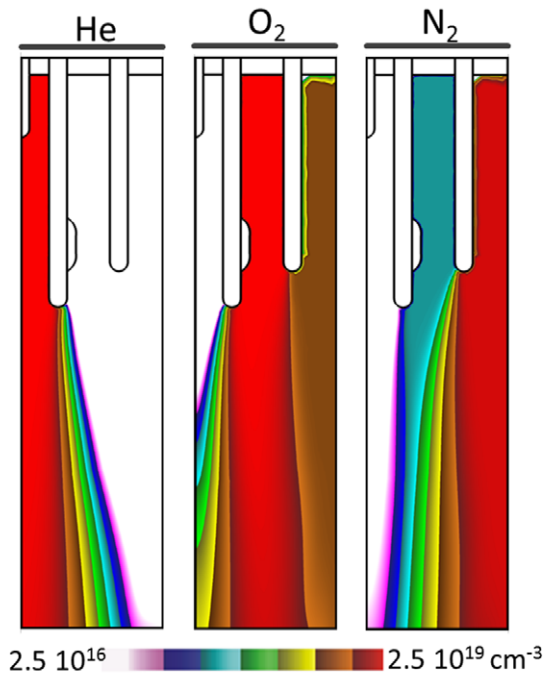


**Figure 12.** Gas composition resulting from the jet flow with  $O_2$  shield gas obtained from the model.

from local chemical processes. The distortion of the discharge indicates a long-range effect. Second, providing  $O_2$  in the downstream region is not sufficient to initiate the backwards directed excitation wave during the positive half-cycle. The backwards directed excitation wave requires that  $O_2$  be present in the vicinity of the jet nozzle.

### 3.4. Modelling of plasma jets with gas shields

The computed densities of He,  $O_2$  and  $N_2$  at 5 ms corresponding to the steady state flow profile for the helium plasma jet with a shielding gas of 99% oxygen and 1% nitrogen are shown in figure 12 prior to the application of a negative voltage at the inner electrode. The sharp demarcation of the central He flow occurs as convective transport strongly dominates diffusive transport into the oxygen shielding gas for the given jet configuration.

Results from the model for the densities of electrons, anions (total of negatively charged ions) and cations (total of positively charged ions) are shown in figure 13 for shielding gases of  $N_2$ ,  $O_2$ , synthetic air and for the e $N_2$  shield gas. The electron impact ionization source and electric field are shown in figure 14. The times of the images (20, 40, 60, and 80 ns) highlight the propagation of the guided negative streamer and the production of associated charged species. The 80 ns image is at the end of the maximum in applied voltage ( $-15$  kV). The electron density inside the tube is basically independent of the composition of the gas curtain. The electrons separate from the powered pin electrode forming a cathode-fall-like sheath and have their highest density at the edge of the sheath. As the electrons drift from the pin electrode in the direction of the grounded ring, they charge the wall of the dielectric tube beneath the ring which produces parallel components of the

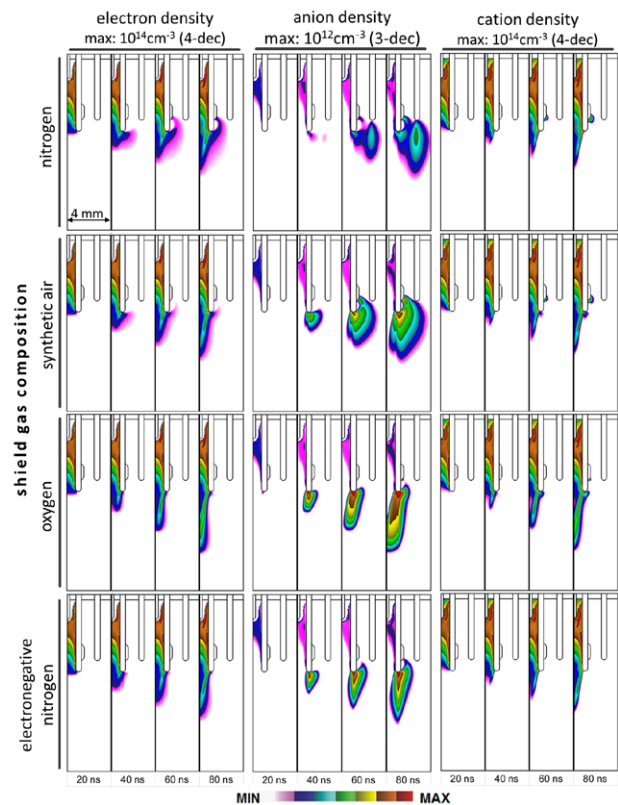


**Figure 13.** Electron, anion and cation density obtained from the numerical model for the indicated shielding gas compositions.

electric field. These parallel components of the electric field sustain a surface ionization wave along the interior wall. This annular plasma density is the source of the annular optical emission observed in previous investigations. The formation of the conducting channel inside the tube compresses the applied voltage into the non-conductive regions outside the plasma channel, and in part helps sustain that ionization wave shown as the source ionization term,  $S_e$ , in figure 14. As the plasma channel approaches the edge of the tube and passes by the grounded electrode outside the tube, the electric field is locally maximum at the end of the tube as shown at 20 ns in figure 14. Also independent of composition of the shielding gas, upon exiting the tube, the ionization wave and plasma density move towards the axis, approximately following the 0.1% contour line of the shielding gas mole fraction. However, the manner in which this transition occurs is sensitive to the shielding gas composition as shown by the propagation of the guided ionization wave into the shielding gas in figure 14.

With the pure  $N_2$  shield gas, the plasma density (represented by the electron density in figure 13) forms a halo around the end of the tube that is absent (or at least greatly diminished) when  $O_2$  is in the shield. The source of the halo is Penning ionization by  $He_m$ , photoionization and diffusion of electrons from the edge of the ionization waves which seeds electrons at larger radii. These electrons then avalanche in the intensified electric field at the edge of the tube. In gas shields containing  $O_2$ , these low energy electrons diffusing or produced by photoionization are quickly consumed to form  $O_2^-$  by 3-body attachment or  $O^-$  by dissociative attachment.

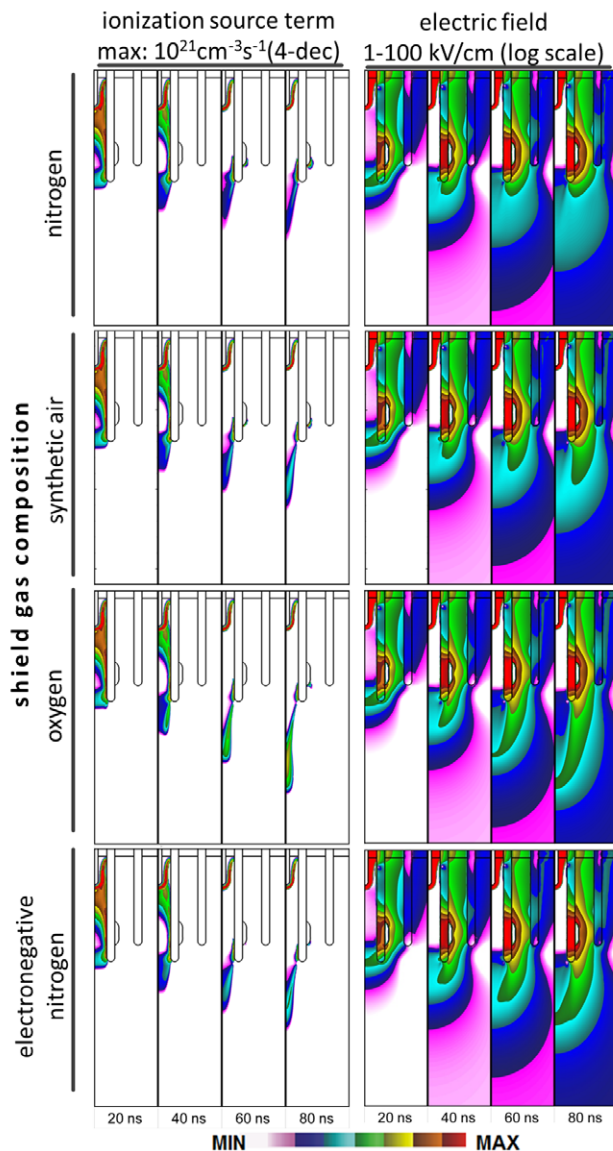


**Figure 14.** Ionization rates and electric field obtained from the model for the indicated shielding gas compositions.

This suppression of the halo is shown by the anion density at the interface between the shield gas and the He plume. This negative ion halo replaces the electron halo produced in the absence of  $O_2$ . Note that with the  $N_2$  shield, there are low densities of anions at the interface between the  $N_2$  shield and surrounding air. This small density of negative ions results from the same processes—dominantly photoionization that seeds electrons in the  $O_2$  containing interface between the air and the  $N_2$  shield.

The length of the electron plume with the  $O_2$  shielding gas is twice as long as for the  $N_2$  shielding gas, 4 mm compared to 2 mm after 80 ns. The on-axis electron density is about an order of magnitude larger for the  $O_2$  shield. The dry air shield is intermediate between the pure gas shields. These densities result from the ionization wave propagating proportionately further with the  $O_2$  shield as shown in figure 14. This further propagation of the ionization wave with the  $O_2$  shield is enabled by an electric field that extends through the low

conductivity of the anion dominated interface between the He plume and the gas shield. The higher conductivity of the interface with the  $N_2$  gas shield shorts out the electric field, and so reduces the magnitude of the ionization wave.

The density of anions is largest with the pure  $O_2$  shield and decreases with the fraction of  $O_2$  in the shield. The sharp demarcation of the anion density at the edge of the tube results from a number of causes. First, the electric field is fairly continuous across the intersection of the He plume and the gas shield while the composition changes over a distance of only a few hundred microns. This change in composition from impure He to  $O_2$  containing molecular gas increases the self-sustaining  $E/N$  (electric field/gas number density) from tens of Td in the He plume to hundreds of Td in the molecular gas. ( $1 \text{ Td} = 10^{-17} \text{ Vcm}^2$  or  $250 \text{ Vcm}^{-1}$  at atmospheric pressure). The self-sustaining  $E/N$  in the molecular gas exceeds that available. The transition between net-ionization and net-attachment across the interface occurs in only  $80 \mu\text{m}$ . Any electrons that are produced at larger radii are quickly attached. With the  $N_2$  shield, the local maximum in anion density at 80 ns below the inner tube results from the 1%  $O_2$  in the  $N_2$  gas shield and the maximum below the outer tube is where the electrons that have spread through the  $N_2$  gas curtain attach to the  $O_2$  in the humid ambient air.

For each composition, the cations follow the electron density with the exception of the lateral spread in the  $N_2$  case. Here the plasma density is below the ambipolar limit in the intense electric fields between the tubes adjacent to the grounded electrons. This allows electrons to rapidly drift independent of the ions but not produce significant ionization.

The higher electric fields obtained for the  $O_2$  containing gas shields are consistent with the proposed mechanisms based on experimental OES measurements. As discussed in section 3.1, the relative change of FNS and SPS emission and the increase in He emission with  $O_2$  content in the shielding suggest higher electric fields in the plasma plume.

The electron plume with the fictitious electronegative  $eN_2$  shield gas closely resembles that for the  $O_2$  shields, having a near complete absence of the electron halo and having the extended electric field enabled by the low conductivity interfacial region. The ionization wave for the  $eN_2$  shield does not extend as far as for the  $O_2$  shield. The vibrational and electronic excitation of  $eN_2$  diffusing into the He plume provides more non-ionizing energy losses for the electrons compared to the  $O_2$  shield. The anion density is lower than in the  $O_2$  shield case, as dissociative attachment is not included for  $eN_2$ .

### 3.5. Electrostatic focusing mechanism (negative half-cycle)

Without  $O_2$  in the shielding gas electrons are transported in radial direction where they excite  $N_2$  at the side of the jet nozzle (see figure 8 phase positions 20–24). The electrons are focused towards the axis when  $O_2$  is present and are able to excite the high energy He and  $N_2$  states. The results from the model (figures 13 and 14) for a negative pulse suggest that  $N_2$  shielding leads to more transport of electrons in the radial direction whereas an electronegative shielding gas is more likely to confine and guide the streamer. As these dynamics

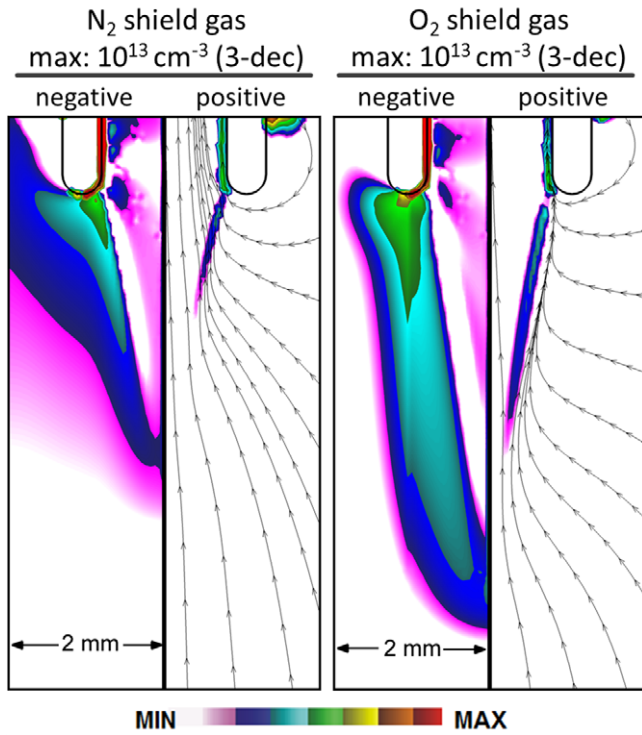


**Figure 15.** Total density of positive and negative charge for  $N_2$  and  $O_2$  shielding gas and electric field lines.

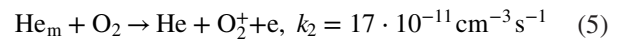
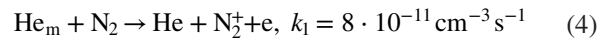
are similar for the  $O_2$  and  $eN_2$  shielded cases, it is likely that the focusing is associated with the electronegativity of the gas.

Based on these observations, an electrostatic focusing mechanism is proposed. The computed positive and negative charge densities in the plasma plume of the jet shielded with  $N_2$  and  $O_2$  are shown in figure 15. The resulting electric field lines (pointing in the opposite direction of electron drift) are also shown. If  $N_2$  is the shield gas, electrons are the primary negative charge carriers. As the streamer head is negatively charged, electrons drift radially outward due to their high mobility. If  $O_2$  shield gas is used, electrons that drift outward are attached to form negative ions that have comparably low mobility. The electric field produced by the anions focuses electrons towards the axis of the jet. In this sense, the negative ions produced by an electronegative shielding gas play a similar role to the charging of the dielectric by electrons for negative streamers propagating inside tubes. In these cases, the surface is charged in front of the streamer head and turns the electric field parallel to the axis of the tube which reinforces the streamer propagation [21]. The second effect of the electronegative gas is the attachment process itself, which prevents ionization waves from propagating outwards in radial direction. In the  $N_2$  shielded case these two confining mechanisms are absent.

This mechanism is consistent with the measurements of OES for an  $N_2$  shield with the additional pipet flow of  $O_2$  and  $N_2$  (see figures 10 and 11). Here the negative space charge with the  $O_2$  injection only acts on one side of the plume. Instead of focusing the ionization wave with attachment on both sides of the channel, the ionization wave migrates towards the other side of the guiding He channel where propagation is less inhibited.

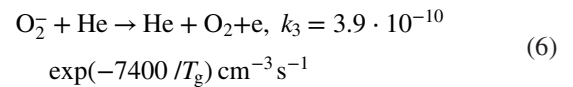
### 3.6. Backwards directed excitation wave (positive half-cycle)

While the mechanisms leading to the backwards directed excitation wave during the positive half-cycle are not yet fully understood, some conclusions can be drawn from our experimental and numerical results. As shown in section 3.3, providing  $O_2$  in the downstream region is not sufficient to produce the backwards directed excitation wave. Consequently, it is also unlikely that photoionization or Penning-ionization of  $O_2$  at the starting point of the backwards directed excitation wave can explain this behavior [38, 39]. The situation is similar for Penning ionization by metastable  $He_m$ , which also has a minor effect on guided streamer propagation [15]. The rate coefficients  $k_i$  for the Penning ionization of  $N_2$  and  $O_2$  [23],

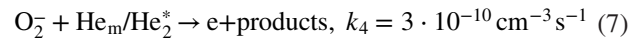


are likely too similar to explain the observed differences. (The same is true for Penning ionization in three-body processes [40]).

Our current hypothesis is that the backwards directed excitation wave depends on the dynamics of the previous negative half-cycle. Anions generated in the downstream region by attachment to  $O_2$  could provide seed electrons through electron detachment reactions for the backwards directed excitation wave in the subsequent positive half-cycle. Electron detachment reactions through thermal reactions such as



are typically important only at temperatures higher than in the plume for our conditions,  $T_g = 350 \text{ K}$  [23], ( $k_3 = 2.6 \cdot 10^{-19} \text{ cm}^3 \text{ s}^{-1}$ ). However, detachment by excited states proceeds with nearly gas kinetic rate coefficients,



In the previous work [23] Winter *et al* measured sufficient metastable densities of  $10^{12} \text{ cm}^{-3}$  at the starting point of the excitation wave before it starts propagating towards the inner pin electrode (1–1.5 mm from the nozzle). Associative attachment producing ozone ( $O_3$ ) from  $O^-$  and  $O_2$  can yield electrons in the plasma plume, as well as the formation of nitrogen oxides in reactions involving  $O^-$  or  $O_2^-$  with typical rate coefficients in the order of  $10^{-10} \text{ cm}^{-3} \text{ s}^{-1}$  [41]. Further modelling and experimental studies using other electronegative shielding gases, would provide additional insights on the origin of the backwards directed excitation wave.

## 4. Concluding remarks

In this work the effects of the composition of the gas shield surrounding a cold atmospheric He plasma jet was investigated both experimentally and numerically. We found that the ratio of optical emission of the first negative system and second positive system of  $N_2$  significantly change depending on whether the shielding gas contains  $O_2$ . Phase resolved

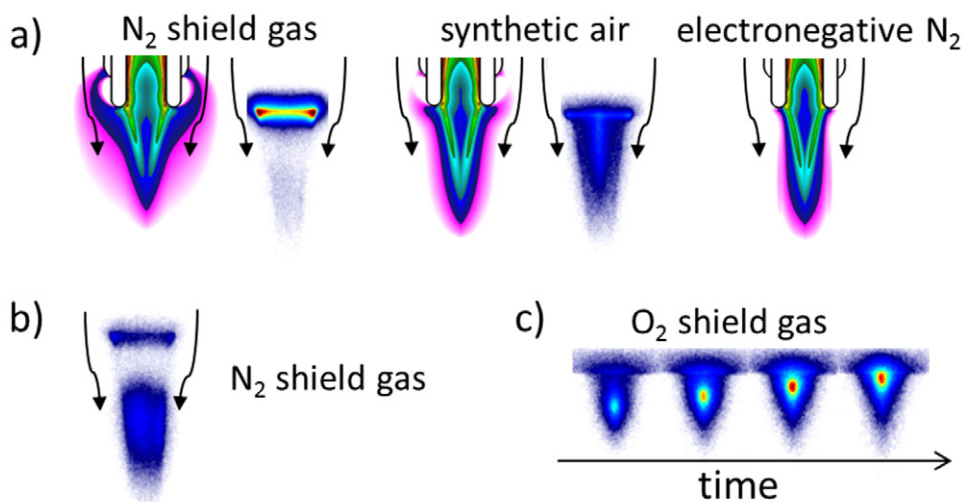


**Figure 16.** Summary illustrating our findings. In (a) the effects of various shielding gas compositions on the propagation of the ionization wave during the negative half-cycle are shown by the electron density obtained from the numerical model and PROES measurements (N<sub>2</sub> emission). If the shielding gas does not contain any O<sub>2</sub>, the ionization wave tends to spread sideways when exiting the tube. The artificial electronegative eN<sub>2</sub> shielding case behaves similar to shielding with synthetic air. In (b) the dark space occurring in the N<sub>2</sub>-shielded jet during the positive half-cycle is shown. In (c) the backwards directed excitation wave occurring during the positive half-cycle of the O<sub>2</sub>-shielded jet is illustrated. (b) and (c) are experimental observations.

optical emission spectroscopy revealed three emission features that are summarized in figure 16: If pure N<sub>2</sub> is used as shielding gas, strong N<sub>2</sub> emission occurs at the side of the jet nozzle during the negative half-cycle. A dark space also occurs close to the exit of the nozzle. If the shielding gas contains O<sub>2</sub>, emission propagates from the ambient towards the jet nozzle against the direction of the gas flow during the positive half-cycle of the jet. From results of modelling, it was found, that when a pure N<sub>2</sub> shielding gas is used, electrons spread radially outward at the edge of the nozzle. This spreading does not occur if the shielding gas contains O<sub>2</sub>. In this case an anion sheath forms around the He channel in which the ionization wave propagates further and produces higher electric fields in the head of the guided streamer. This is due to the lower conductivity outside the core of the guided streamer that enables greater penetration of the electric field.

Based on these experimental and numerical findings, the following mechanism is proposed. The electric field generated by the anions contributes to a focusing of the electrons towards the center of the He channel, thereby promoting the propagation of the ionization wave during the negative half-cycle. In this way anions can be generated at distances of a few mm from the jet nozzle. These anions can then provide the seed electrons for the backwards directed excitation wave observed during the next positive half-cycle. This mechanism is consistent with the behavior of the jet when injecting O<sub>2</sub> with a pipette. The injected O<sub>2</sub> focuses the ionization wave to the opposite side of the He channel from where the gas is injected. Electrostatic forces due to negative space charge caused by anions can have a significant effect on the propagation of guided streamers in cold atmospheric pressure plasma jets operated with noble gases. The observed effects appear to arise from the interface of a non-electronegative and an electronegative gas. Through a variation of the shield gas composition fundamental plasma parameters (plasma density, mean electron energy) in the plasma plume of

CAPJ can be influenced. This can be exploited for the optimization of plasma processes for the typical fields of application of such devices, e.g. for the treatment of biotechnological surfaces or biological tissue.

## Acknowledgments

The work of A Schmidt-Bleker, J Winter, S Reuter and K-D Weltmann was funded by the German Federal Ministry of Education and Research (Grant No 03Z2DN12). The work of S Norberg and M J Kushner was supported by the United States Department of Energy Office of Fusion Energy Science (DE-SC0001319) and the National Science Foundation (CHE-1124724).

## References

- [1] Ehlbeck J, Schnabel U, Polak M, Winter J, Von Woedtke T, Brandenburg R, Von dem Hagen T and Weltmann K 2011 Low temperature atmospheric pressure plasma sources for microbial decontamination *J. Phys. D: Appl. Phys.* **44** 013002
- [2] Park G, Park S, Choi M, Koo I, Byun J, Hong J, Sim J, Collins G and Lee J 2012 Atmospheric-pressure plasma sources for biomedical applications *Plasma Sources Sci. Technol.* **21** 043001
- [3] von Woedtke T, Reuter S, Masur K and Weltmann K-D 2013 Plasmas for medicine *Phys. Rep.* **530** 291–320
- [4] Lu X, Laroussi M and Puech V 2012 On atmospheric-pressure non-equilibrium plasma jets and plasma bullets *Plasma Sources Sci. Technol.* **21** 034005
- [5] Lu X, Naidis G, Laroussi M and Ostrikov K 2014 Guided ionization waves: theory and experiments *Phys. Rep.* **540** 123–66
- [6] Reuter S, Winter J, Schmidt-Bleker A, Tresp H, Hammer M U and Weltmann K-D 2012 Controlling the ambient air affected reactive species composition in the effluent of an argon plasma jet *IEEE Trans. Plasma Sci.* **40** 2788–94

- [7] Schmidt-Bleker A, Winter J, Iseni S, Dünnbier M, Weltmann K and Reuter S 2014 Reactive species output of a plasma jet with a shielding gas device—combination of FTIR absorption spectroscopy and gas phase modelling *J. Phys. D: Appl. Phys.* **47** 145201
- [8] Reuter S, Winter J, Schmidt-Bleker A, Schroeder D, Lange H, Knake N, Gathen V S-v d and Weltmann K-D 2012 Atomic oxygen in a cold argon plasma jet: TALIF spectroscopy in ambient air with modelling and measurements of ambient species diffusion *Plasma Sources Sci. Technol.* **21** 024005
- [9] Barton A 2014 Impact of non-thermal plasma on cell signaling in keratinocytes *PhD Thesis* Ernst-Moritz-Arndt-Universität Greifswald, Germany
- [10] Zhu W-C, Li Q, Zhu X-M and Pu Y-K 2009 Characteristics of atmospheric pressure plasma jets emerging into ambient air and helium *J. Phys. D Appl. Phys.* **42** 202002
- [11] Hofmann S, Sobota A and Bruggeman P 2012 Transitions between and control of guided and branching streamers in dc nanosecond pulsed excited plasma jets *IEEE Trans. Plasma Sci.* **40** 2888–99
- [12] Breden D, Miki K and Raja L 2012 Self-consistent two-dimensional modeling of cold atmospheric-pressure plasma jets/bullets *Plasma Sources Sci. Technol.* **21** 034011
- [13] Sakiyama Y and Graves D B 2009 Neutral gas flow and ring-shaped emission profile in non-thermal RF-excited plasma needle discharge at atmospheric pressure *Plasma Sources Sci. Technol.* **18** 025022
- [14] Goree J, Liu B, Drake D and Stoffels E 2006 Killing of S. mutans bacteria using a plasma needle at atmospheric pressure *IEEE Trans. Plasma Sci.* **34** 1317–24
- [15] Naidis G 2011 Modelling of plasma bullet propagation along a helium jet in ambient air *J. Phys. D Appl. Phys.* **44** 215203
- [16] Naidis G 2010 Modelling of streamer propagation in atmospheric-pressure helium plasma jets *J. Phys. D Appl. Phys.* **43** 402001
- [17] Boeuf J-P, Yang L L and Pitchford L C 2013 Dynamics of a guided streamer ('plasma bullet') in a helium jet in air at atmospheric pressure *J. Phys. D: Appl. Phys.* **46** 015201
- [18] Babaeva N Y and Kushner M J 2014 Interaction of multiple atmospheric-pressure micro-plasma jets in small arrays: He/O<sub>2</sub> into humid air *Plasma Sources Sci. Technol.* **23** 015007
- [19] Naidis G 2011 Simulation of streamers propagating along helium jets in ambient air: polarity-induced effects *Appl. Phys. Lett.* **98** 141501
- [20] Jiang C, Chen M and Gundersen M 2009 Polarity-induced asymmetric effects of nanosecond pulsed plasma jets *J. Phys. D: Appl. Phys.* **42** 232002
- [21] Xiong Z, Robert E, Sarron V, Pouvesle J-M and Kushner M J 2013 Atmospheric-pressure plasma transfer across dielectric channels and tubes *J. Phys. D: Appl. Phys.* **46** 155203
- [22] Luque A, Ratushnaya V and Ebert U 2008 Positive and negative streamers in ambient air: modelling evolution and velocities *J. Phys. D: Appl. Phys.* **41** 234005
- [23] Winter J, Sousa J S, Sadeghi N, Schmidt-Bleker A, Reuter S and Puech V 2015 The spatio-temporal distribution of He (<sup>2</sup>S<sub>1</sub>) metastable atoms in a MHz-driven helium plasma jet is influenced by the oxygen/nitrogen ratio of the surrounding atmosphere *Plasma Sources Sci. Technol.* **24** 025015
- [24] Dünnbier M, Schmidt-Bleker A, Winter J, Wolfram M, Hippler R, Weltmann K and Reuter S 2013 Ambient air particle transport into the effluent of a cold atmospheric-pressure argon plasma jet investigated by molecular beam mass spectrometry *J. Phys. D: Appl. Phys.* **46** 435203
- [25] Lay B, Moss R S, Rauf S and Kushner M J 2003 Breakdown processes in metal halide lamps *Plasma Sources Sci. Technol.* **12** 8
- [26] Xiong Z and Kushner M J 2012 Atmospheric pressure ionization waves propagating through a flexible high aspect ratio capillary channel and impinging upon a target *Plasma Sources Sci. Technol.* **21** 034001
- [27] Norberg S A, Johnsen E and Kushner M J 2015 Formation of reactive oxygen and nitrogen species by repetitive negatively pulsed helium atmospheric pressure plasma jets propagating into humid air *Plasma Sources Sci. Technol.* Accepted for publication
- [28] Lofthus A and Krupenie P H 1977 The spectrum of molecular nitrogen *J. Phys. Chem. Ref. Data* **6** 113–307
- [29] Brooks R and Hunt J 1988 Helium emission spectra from doped samples of solid hydrogen and deuterium *J. Chem. Phys.* **88** 7267–72
- [30] Kramida A, Yu R and Reader J and NIST ASD Team 2014 *NIST Atomic Spectra Database (version 5.2)* (Gaithersburg, MD: National Institute of Standards and Technology)
- [31] Winter J, Wende K, Masur K, Iseni S, Dünnbier M, Hammer M, Tresp H, Weltmann K and Reuter S 2013 Feed gas humidity: a vital parameter affecting a cold atmospheric-pressure plasma jet and plasma-treated human skin cells *J. Phys. D: Appl. Phys.* **46** 295401
- [32] Gerling T, Nastuta A, Bussiahn R, Kindel E and Weltmann K 2012 Back and forth directed plasma bullets in a helium atmospheric pressure needle-to-plane discharge with oxygen admixtures *Plasma Sources Sci. Technol.* **21** 034012
- [33] Iseni S, Schmidt-Bleker A, Winter J, Weltmann K and Reuter S 2014 Atmospheric pressure streamer follows the turbulent argon air boundary in a MHz argon plasma jet investigated by OH-tracer PLIF spectroscopy *J. Phys. D: Appl. Phys.* **47** 152001
- [34] Schmidt-Bleker A, Reuter S and Weltmann K-D 2014 Non-dispersive path mapping approximation for the analysis of ambient species diffusion in laminar jets *Phys. Fluids* **26** 083603 (1994-present)
- [35] Hagelaar G and Pitchford L 2005 Solving the Boltzmann equation to obtain electron transport coefficients and rate coefficients for fluid models *Plasma Sources Sci. Technol.* **14** 722
- [36] Biagi-v7.1 database, [www.lxcat.net](http://www.lxcat.net), retrieved on October 1, 2014
- [37] Phelps database, [www.lxcat.net](http://www.lxcat.net), retrieved on October 1, 2014
- [38] Kurunczi P, Lopez J, Shah H and Becker K 2001 Excimer formation in high-pressure microhollow cathode discharge plasmas in helium initiated by low-energy electron collisions *Int. J. Mass Spec.* **205** 277–83
- [39] Huebner W F and Mukherjee J 2014 Photoionization and photodissociation rates in solar and blackbody radiation fields *Planetary and Space Science* **106** 111–45
- [40] Myers G and Cunningham A J 1977 Quenching reactions of He(2<sup>3</sup>S) and He2(2<sup>3</sup>Σ) metastables in the presence of N<sub>2</sub> and O<sub>2</sub> *J. Chem. Phys.* **67** 3352–9
- [41] Murakami T, Niemi K, Gans T, O'Connell D and Graham W G 2013 Chemical kinetics and reactive species in atmospheric pressure helium–oxygen plasmas with humid-air impurities *Plasma Sources Sci. Technol.* **22** 015003